



# JGR Space Physics

## RESEARCH ARTICLE

10.1029/2020JA028014

# Quantification of the Atmospheric Relativistic Electron Precipitation on 17 January 2013

S. Shekhar<sup>1,2</sup> , R. M. Millan<sup>1</sup>, L. A. Woodger<sup>1</sup>, and M. Qin<sup>1</sup> 

<sup>1</sup>Department of Physics and Astronomy, Dartmouth College, Hanover, NH, USA, <sup>2</sup>Department of Physics, Auburn University, Auburn, AL, USA

### Key Points:

- A net atmospheric loss of 5% of the >700-keV radiation belt particles was obtained between 2:44 to 15:04 UT (~13.5 h) on 17 January 2013
- Nearly 75% of atmospheric loss was prestorm occurring through six REP events (average of ~12% per REP event)
- One REP event during the onset of the storm caused ~25% of atmospheric loss and was followed by flux dropouts during the main phase

### Correspondence to:

S. Shekhar,  
szs0230@auburn.edu

### Citation:

Shekhar, S., Millan, R. M., Woodger, L. A., & Qin, M. (2020). Quantification of the atmospheric relativistic electron precipitation on 17 January 2013. *Journal of Geophysical Research: Space Physics*, 125, e2020JA028014. <https://doi.org/10.1029/2020JA028014>

Received 15 MAR 2020

Accepted 10 JUL 2020

Accepted article online 11 AUG 2020

**Abstract** On 17 January 2013, relativistic electron precipitation (REP) was observed on Balloon Array for Radiation Belt Relativistic Electron Losses (BARREL) payloads, National Oceanic and Atmospheric Administration Polar orbiting Operational Environmental Satellites (NOAA POES), and European Space Agency (ESA) MetOp between 2:44 to 15:04 h UT, scattered across dusk to early morning magnetic local time (MLT) sectors. The observations could be grouped into multiple observations of seven REP events spatially separated by more than 2 h in MLT and at least 1 h in UT. Almost all the events were localized in L shell with  $dL < 0.5$  and MLT with  $dMLT < 3$ . A net loss of ~5% of the relativistic electrons from the radiation belts is estimated between 2:44 to 15:04 h UT (~13.5 h). A majority of atmospheric REP (nearly 75% through six REP events) was observed before the onset of a minor storm around 14:00 UT; the rest (25% through one REP event) was observed during the commencement of the storm which was followed by a major dropout of MeV electrons from the radiation belts during the main phase. However, no atmospheric precipitation was observed during the main phase, indicating that the dropouts may not have been caused by particle loss into the atmosphere.

## 1. Introduction

Relativistic electrons in the radiation belts affect space technology and are hence an important aspect of space weather. The loss of electrons into the atmosphere, known as precipitation, is important for radiation belt dynamics. Previous studies have indicated that spatial scales (e.g., Shekhar et al., 2017) and energy spectra (e.g., Comess et al., 2013; Shekhar et al., 2018; Smith et al., 2016) vary with L and magnetic local time (MLT) locations and hence may be closely tied to the mechanism involved.

Particle fluxes in the outer radiation belt can be reduced by the reconfiguration of magnetic field while conserving the adiabatic invariants. Such a loss is recovered when the magnetic field configuration is restored, and hence, such processes (e.g., Dst effect and adiabatic localized tail-like stretching of magnetic field) do not produce a permanent loss (e.g., Fillius & McIlwain, 1967; Lee et al., 2006; Onsager et al., 2002). Processes such as the magnetopause shadowing effect, wave-particle interactions, and nonadiabatic localized tail-like stretching of magnetic field can produce a permanent loss of particles (e.g., Lee et al., 2006; Onsager et al., 2002; Young et al., 2002). In the case of the magnetopause shadowing effect, as the particles encounter the magnetopause during their drift motion, relativistic electrons are lost into the magnetosheath. Due to magnetic field stretching and wave-particle interactions, the electrons are lost into the BLC and precipitate into the atmosphere. Thus, low-altitude observations of relativistic electron precipitation (REP), such as those by low Earth orbiting satellites like the National Oceanic and Atmospheric Administration Polar orbiting Operational Environmental Satellites (NOAA POES) and European Space Agency (ESA) MetOp, can be used to distinguish these mechanisms.

In previous studies, REP events have been found to extend from tens of minutes to hours (Millan et al., 2002) and statistically confined to L shell widths of 0.5 and MLT widths of 3 h (Shekhar et al., 2017). The spatial extent and duration of the precipitation may depend on the spatial distribution and the duration of the mechanism causing the energy transfer leading to the scattering of particles in the loss cone. Electromagnetic ion cyclotron (EMIC) waves have been found to resonantly scatter MeV electrons from the radiation belts (e.g., Li et al., 2014; Lyons & Thorne, 1972; Miyoshi et al., 2008; Summers & Thorne, 2003; Ukhorskiy et al., 2010; Woodger et al., 2018). Recently Capannolo et al. (2019) showed, through analysis of three geomagnetic storms coincident with EMIC wave activity on RBSP spacecrafts, that REP was latitudinally localized but

**Table 1**  
*BARREL X-Ray Data Products*

X-ray data product	Energy range (keV)	Channels	Time resolution
Fast spectra	FSPC1 = 25–180	4	50 ms
	FSPC2 = 180–550		
	FSPC3 = 550–840		
	FSPC4 = 840–1,500		
Medium spectra	100–4,000	48	4 s
Slow spectra	25–10,000	256	32 s

could occur in different locations within a rather broad L-MLT region (up to  $\sim 1.4$  L shells and  $\sim 4.4$  h MLT). However, the contribution of EMIC waves toward global precipitation of electrons from the radiation belts remains unexplored. A few efforts in this direction are being made through estimation of the spatial scale of EMIC waves and REP (e.g., Blum et al., 2017; Capannolo et al., 2019; Shekhar et al., 2017).

Previously, a few case studies like Blum et al. (2013) and Zhang et al. (2017) focused on spatial scales of precipitation and quantified the electron loss for an REP event on 18–19 January 2013 observed in proximity to EMIC waves. They used observations from 17 January 2013, relativistic electron precipitation (REP) was observed on Balloon Array for Radiation Belt Relativistic Electron Losses (BARREL) payloads and Colorado Student Space Weather Experiment (CSSWE) CubeSat. Millan et al. (2002) quantified MeV precipitation events observed on MeV Auroral X-ray Imaging and Spectroscopy (MAXIS) balloon payload detected between magnetic latitudes  $58^\circ$  to  $68^\circ$  (L values of 3.8–6.7) but only in the late afternoon/dusk sectors (14:30–00:00 MLT). Quantification of observed precipitation is limited by sparse spatial data, and hence, POES/MetOp data, with better spatial resolution, could be useful in estimation of observational loss of relativistic electrons from the radiation belts. The statistical study by Shekhar et al. (2017) used multiple POES/MetOp satellites to explore the variations of spatial scales of REP. They found that REP events separated into two different classes of events with different spatial scales ( $dL \leq 0.5$ ,  $dMLT \leq 3$  h;  $1 \leq dL \leq 2.5$ ,  $dMLT \leq 3$  h) which also varied in their locations of maximum occurrence probabilities. Some studies have also used satellite data in models to quantify electron loss from the radiation belts. Based on SAMPEX/PET observations, Tu et al. (2010) quantified electron loss to the atmosphere in the Earth's radiation belt using a drift diffusion model that includes the effects of azimuthal drift and pitch angle diffusion. Pham et al. (2017) used the same model to quantify loss based on POES/MetOp data, increasing the spatial and temporal resolution due to the presence of multiple POES satellites. However, POES/MetOp has not been used to observationally quantify particle loss.

In this study, we used POES/MetOp and BARREL payloads to observe REP over the entire day on 17 January 2013. We found REP events during time intervals after 10:00 UT which had not been published before. With the availability of modeled electron precipitation spectra for the time periods 3:00 and 4:50 UT from Li et al. (2014) and Woodger et al. (2018), respectively, and good spatial coverage due to the availability of POES/MetOp and BARREL payloads, this was a good day for estimation of electron loss observationally. Interestingly, POES/MetOp also observed precipitation in the morning local time sector which is not very typical. Previous balloon payloads such as MAXIS (Millan et al., 2002) and BARREL (Millan et al., 2013) and recent observations on the Calorimetric Electron Telescope at International Space Station (Kataoka et al., 2016) observed REP events mainly at the dusk to midnight sector.

## 2. Data Sets Used

REPs were observed in BARREL balloon payloads as well as POES/MetOp satellites. BARREL is an array of stratospheric balloons carrying scintillation detectors which measure bremsstrahlung X-rays from the precipitation of radiation belt electrons into the atmosphere (Millan et al., 2013). The data used in this study are taken from the austral summer 2013 campaign which was conducted from SANAE and Halley VI stations in the Southern Hemisphere. The energy channels are listed in Table 1. The REP events in BARREL payloads were identified by elevated X-ray count rates extending to the FSPC3 channel (550–840 keV) that were 3 sigma (standard deviation) above background determined through a sliding window. Then, any

**Table 2**  
POES/MetOp MEPED Channels (Yando et al., 2011)

Channel	Energy range of electrons response (keV)	Energy range of protons response (keV)
E1	>30	210–2,700
E2	>100	280–2,700
E3	>300	440–2,700
P1	Negligible	30–80
P2	Negligible	80–250
P3	Negligible	250–800
P4	Negligible	800–2,500
P5	Negligible	2,500–7,000
P6	>700	>7,000

selected events that were not REP such as gamma ray bursts (GRBs) were removed through inspection by eye (Woodger et al., 2015).

The POES network of polar orbiting spacecraft is operated by NOAA while MetOp is operated by EUMETSAT. These satellites (NOAA-15, NOAA-16, NOAA-17, NOAA-18, NOAA-19, MetOp-01, MetOp-02) occupy sunsynchronous polar orbits (typical parameters: nominal altitude 870 km, orbital period 102 min, inclination 98.7°) and are three-axis stabilized such that their orientation is fixed relative to the direction of travel and the local zenith with the MEPED (Medium Energy Proton Electron Detector) 0° telescopes pointing to the local zenith and MEPED 90° telescopes pointing in a perpendicular direction relative to it (Yando et al., 2011). MEPED has two pairs of directional telescopes (0° and 90°) and four omnidirectional detectors. The directional telescopes have a ±15° field of view and the omnidirectional detectors have ±60° field of view. In this study, the 0° directional telescopes have been used as at high latitudes, they detect particles that are in the bounce loss cone (BLC) (Rodger et al., 2010). Table 2 shows the detector response for electrons and protons over a range of energies (Yando et al., 2011). When P5 channel does not record any counts but P6 does, it means that P6 is recording contaminating electrons with energies >700 keV. In this way, P5 and P6 channels can be used to identify REP events.

Locations of REP observed on  
POES/MetOp (squares) and BARREL payloads (circles)  
on 17th January 2013

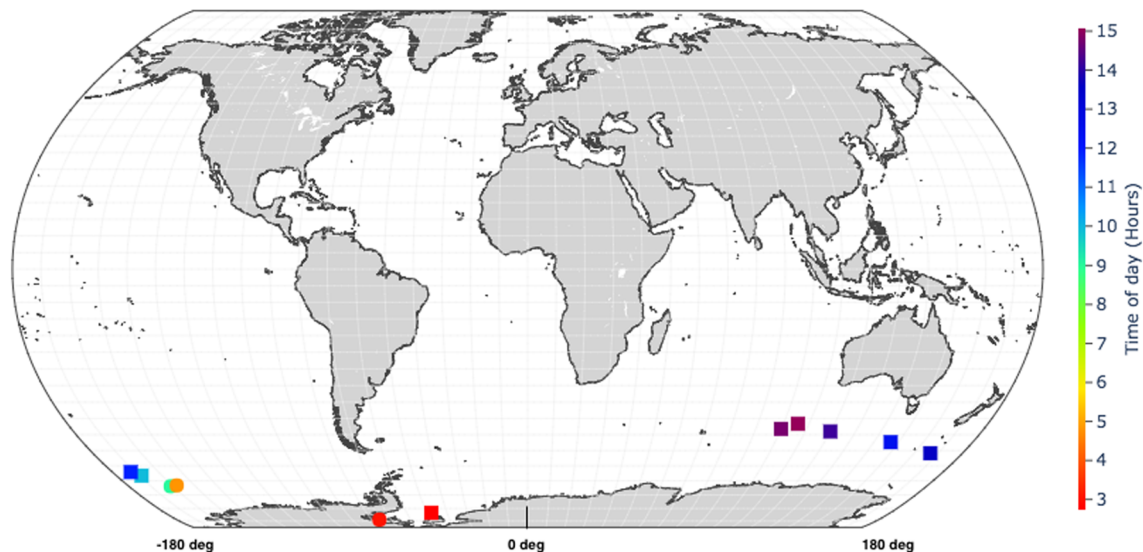


**Figure 1.** All POES/MetOp and BARREL observations of REP on 17 January 2013. All the precipitation was observed in the Southern Hemisphere. The location of observed events appears to drift westward in time.

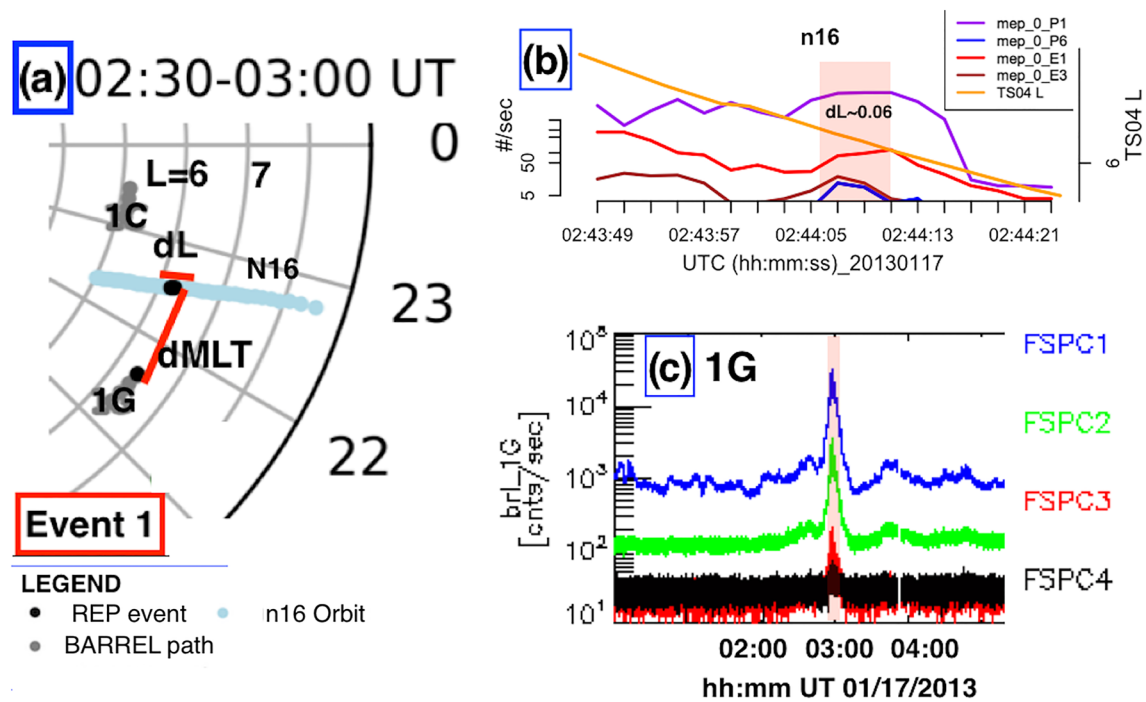


**Figure 2.** (a) L-MLT locations of all POES/MetOp spacecraft and BARREL payloads between 2:30 to 3:00 UT. Sun is located to the left. Locations are shown for the times of REP observation and POES orbits in the Southern Hemisphere. The region of precipitation was marked by dL and dMLT highlighted in red. (b) Count rates observed in NOAA-16. dL or L shell width is calculated as the count rates in the P6 channel elevate to  $>5$  c/s. (c) BARREL fast spectra observed on payload 1G. Elevated count rates are observed extending to the FSPC3 channel at 3:00 UT. A REP event in BARREL payload is defined as count rates in FSPC3 channel extending to values  $>3$  times the standard deviation in the count rates.

The location and time of events on POES and MetOp were obtained from the list of events by Shekhar et al. (2017), which used 16-s resolution data. However, we used 2-s count rate data here to define the spatial extent.

### 3. REP Observations

Between 2:44 to 15:04 UT, several REP events were observed in the dusk to postmidnight sectors by several POES and MetOp satellites and BARREL payloads. Figure 1 shows all the locations where REP events were observed by BARREL payloads and POES/MetOp. All the precipitation was observed in the Southern Hemisphere. It is notable that the location of observed events appears to drift westward in time (also observed in Figures 2–7), reflecting the fact that REP occurs primarily at the dusk to postmidnight sectors.

#### 3.1. L-MLT Locations of REPs

POES/MetOp record energetic precipitation at eight different times which are observed as spikes at least  $>5$  c/s in the P6 channel count rates. The L shell and MLT locations were obtained through mapping using the TS04 magnetic field model. Payload 1G observed intense energetic electron precipitation around 3:00 UT (Figure 2c) while II observed energetic electron precipitation around 4:50 UT (Figure 3b) and between 8:30 to 9:15 UT (Figure 4b). Payloads 1C, 1K, and 1O did not observe any precipitation.

In order to quantify loss, we needed to define a region in which REP event could be assumed to be confined. For some REP events, precipitation was observed at more than one location, and in such cases, the region was simply defined as the region enclosed by the two observations. For some REP events, precipitation was observed at only one location. In such cases, we confined the REP events using the nearest observation of the absence of REP within the maximum MLT extent of REP events,  $dMLT < 3$  h defined by Shekhar et al. (2017). This may lead to an overestimation of the region of precipitation. However, Shekhar et al. (2017) had found that the REP events were so localized that they were observed in only one satellite in a spatially arranged constellation of all POES/MetOp satellites in almost 99% of the cases. As such, our estimate is restricted by the spatial resolution available for a particular event. If there were two satellite passes enclosing

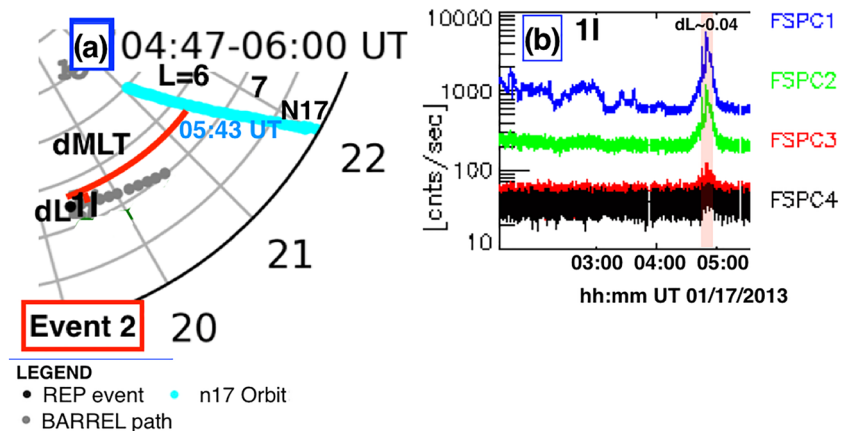


**Figure 3.** (a) L-MLT locations of all POES/MetOp spacecraft and BARREL payloads between 4:47 to 6:00 UT. Sun is located to the left. Locations are shown for the times of REP observation and POES orbits in the Southern Hemisphere. NOAA-17 passes nearest to the payload 1I at ~5:43 UT confining the event in MLT. The region of precipitation was marked by dL and dMLT highlighted in red. (b) BARREL fast spectra observed on payload 1I. Elevated count rates are observed extending to the FSPC3 channel at 4:50 UT. dL is measured by the drifting balloon as it sees precipitation.

the location where REP was observed and they were separated in MLT by less than 3 h, both the passes were used to confine the region of precipitation.

As shown in Figures 2b and 2c, the first observation made by NOAA-16 at 2:44 UT is observed about 16 min before BARREL payload 1G sees it. It was very close to the location where BARREL payloads observed the precipitation (Figure 2a). The MLT separation between BARREL 1G and NOAA-16 is 0.85 h which is within the spatial scale of REP events found by Shekhar et al. (2017) and are hence assumed to be the same event. The two observations are collectively labeled as Event 1.

BARREL payload 1I observed energetic precipitation around 4:50 UT (as shown in Figure 3b). NOAA-17 (shown in blue in Figure 3a) made a pass in the Southern Hemisphere around 5:43 UT closest in L and MLT as BARREL payload 1I but did not observe precipitation. This BARREL observation was labeled Event 2, and it was assumed to extend in MLT as far as NOAA-17 pass around the L shell at which event was observed by 1I.

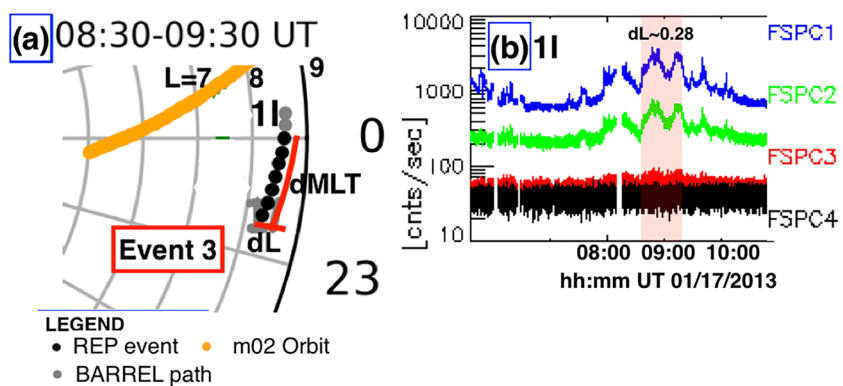


**Figure 4.** (a) L-MLT locations of all POES/MetOp spacecraft and BARREL payloads between 8:30 to 9:30 UT. Sun is located to the left. Locations are shown for the times of REP observation and POES orbits in the Southern Hemisphere. The region of precipitation was measured by the drifting balloon as payload 1I saw precipitation and was marked by dL and dMLT highlighted in red. (b) BARREL fast spectra observed on payload 1I. Elevated count rates are observed extending to the FSPC3 channel between 8:30 to 9:15 UT and have a data gap around 8:10 UT. Therefore, the temporal extent of that event was restricted to the times when the data were available

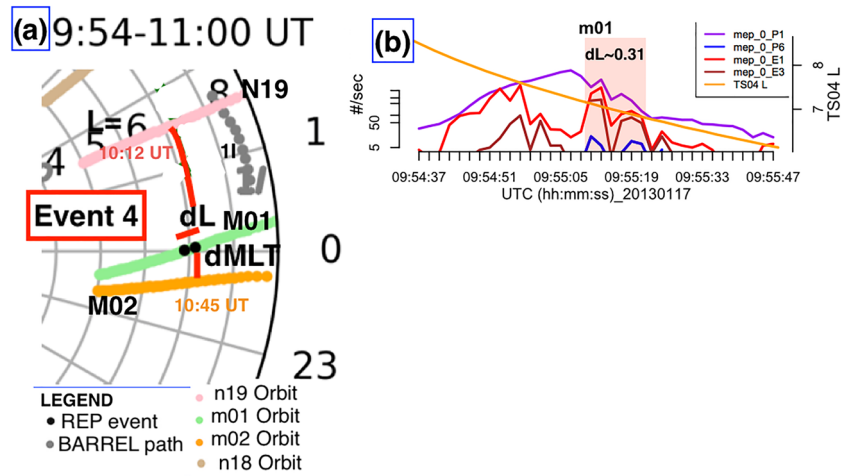


**Figure 5.** (a) L-MLT locations of all POES/MetOp spacecraft and BARREL payloads between 9:54 to 11:00 UT. Sun is located to the left. Locations are shown for the times of REP observation and POES orbits in the Southern Hemisphere. dL was estimated from MetOp-01 at 9:55 UT. dMLT was estimated using two nearest satellite passes by NOAA-19 at 10:12 UT and MetOp-02 at 10:45 UT enclosing MetOp-01. Both are highlighted in red. (b) Precipitation (blue) is observed on MetOp-01, and dL is measured as the satellite moves across L shell (yellow).

BARREL payload 11 observed energetic precipitation between 8:30 to 9:15 UT (Figure 4b). Payload 11 drifted slightly in L shell and MLT, and the extent of this event was determined solely by its drift as it observed precipitation. This was labeled as Event 3.

The location of the observation made by MetOp-01 at 9:55 UT (Figure 5b) is shown in Figure 5a. It is enclosed by MetOp-02 which passes by closest in L and MLT at around 10:45 UT and NOAA-19 which passes by around 10:12 UT but do not observe precipitation. They are separated in MLT by 1.95 h. The three observations were collectively labeled Event 4.

Figure 6a shows the next set of POES observations between 11:30 to 13:40 UT. NOAA-19 observed REP twice in the postmidnight sector at 11:54 and 13:35 UT (Figures 6b and 6c). Both of the postmidnight observations were collectively labeled Event 5 in this study. In the evening to midnight sector, MetOp-02 observed REP at 12:27 UT (Figure 6d) with two passes of MetOp-01, at 11:39 and 13:21 UT, enclosing it (Figure 6a). This observation is labeled as Event 6 in this study. Though Event 6 occurred around the same time as Event 5, they were separated by dMLT  $\sim 3$ , indicating that they may have been different events as the spatial scale of REP was found to be dMLT  $< 3$  in the study by Shekhar et al. (2017).

Figure 7a shows the next set of POES/MetOp observations between 14:05 to 15:05 UT. MetOp-02, NOAA-16, and MetOp-01 observed precipitation at 14:09, 14:46, and 15:04 UT, respectively (Figures 7b to 7d). The maximum MLT separation between the satellites is  $\sim 1.09$ , and there were no POES/MetOp passes showing absence of precipitation to separate the three observations. These three observations were labeled Event 7 in this study.

## 4. Quantification of Loss

### 4.1. Flux Calculations

Since  $0^\circ$  MEPED POES/MetOp channels measure BLC particle count rates, we use geometric factors  $G$  defined by Yando et al. (2011) to convert them into fluxes. For electron energies  $> 700$  keV,  $G$  in the P6 channel was almost constant with  $G = 0.01 \text{ cm}^{-2} \text{ sr}^{-1}$ . Hence, flux  $\Delta f_{\text{poes}}$  is given by

$$\Delta f_{\text{poes}} = \frac{P6_{\text{counts}}}{G} \quad (1)$$

To obtain flux from BARREL payloads, we used the electron spectra from the quasilinear simulations by Li et al. (2014) for the observation at 3:00 UT, by Woodger et al. (2018) for the observation at 4:50 UT, and an exponential best fit electron spectrum for 8:15–9:30 UT observation represented by  $F$  as a function of energy

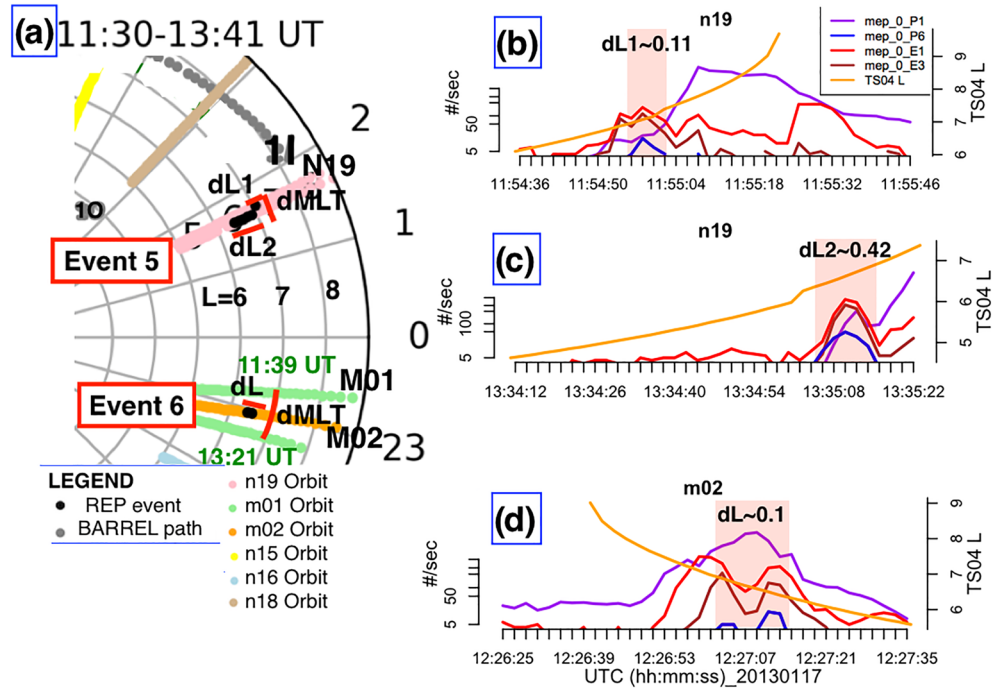


**Figure 6.** (a) L-MLT locations of all POES/MetOp spacecraft and BARREL payloads between 11:30 to 13:41 UT. Sun is located to the left. Locations are shown for the times of REP observation and POES orbits in the Southern Hemisphere. Event 5 was observed in the postmidnight sector. The region of precipitation was confined by two consecutive NOAA-19 REP observations. Event 6 is observed by MetOp-02 at 12:27 UT in the premidnight sector and is confined by two nearest MetOp-01 passes at 11:39 and 13:21 UT. The L and MLT extent estimated for both the events is marked in red. (b, c) NOAA-19 REP observations for Event 5. REP is observed at 11:54 and 13:35 UT. (d) MetOp-02 REP observation constituting Event 6. dL is measured as the satellite moves across L shell and sees precipitation.

$E$  in Equation 2. The spectrum in each case was integrated over energies of 700 keV to 10 MeV to obtain flux ( $\Delta f_{barrel}$ ) as shown in Equation 2.

$$\Delta f_{barrel} = \int_{700keV}^{10MeV} F(E)dE \quad (2)$$

#### 4.2. Region of Precipitation

Figures 2–7 show the L-MLT locations of all REP events. In each plot, the dL and dMLT which correspond to the L shell and MLT extent of the event are shown. As summarized in Table 3, seven different sets of precipitation events were observed between 2:44 to 15:04 UT on 17 January 2013. The event start and end latitudes/longitudes are also shown in Table 3. For BARREL, the altitude was assumed to be 100 km where precipitation of electrons is expected. For all the POES/MetOp observations, POES/MetOp altitude was used to determine the area of the region of precipitation. We use spherical coordinate system to define an area element  $dA$  at altitude  $h$ .

$$\int_{prec.region} dA = 2.\pi. \int_{\phi_{start}}^{\phi_{end}} \int_{\theta_{start}}^{\theta_{end}} (R_E + h). \cos(\theta_{lat}).d(\phi_{lon}).(R_E + h).d(\theta_{lat}) \quad (3)$$

$$A = |2.\pi.(R_E + h)^2.(\sin(\theta_{end}) - \sin(\theta_{start})).(\phi_{end} - \phi_{start})| \quad (4)$$

where  $A$  is the area of the region of precipitation altitude  $h$ ,  $R_E$  is the radius of Earth, and  $\theta_{start/end}$  and  $\phi_{start/end}$  are the latitudes and longitudes of the starting/ending locations of the REP, respectively. The calculated areas are listed in column 4 of Table 3. In some cases, two POES/MetOp satellites estimated two different L shell extents at two different locations. As such, we determined the region of precipitation as the areas covered by each POES/MetOp satellite with the dL measured by the individual satellite and dMLT measured by the separation between the two satellites. Hence, we labeled the different regions corresponding to each set of dL and dMLT as shown in Figures 2–7. Event 7 (Figure 7a) consisted of three different dLs at three

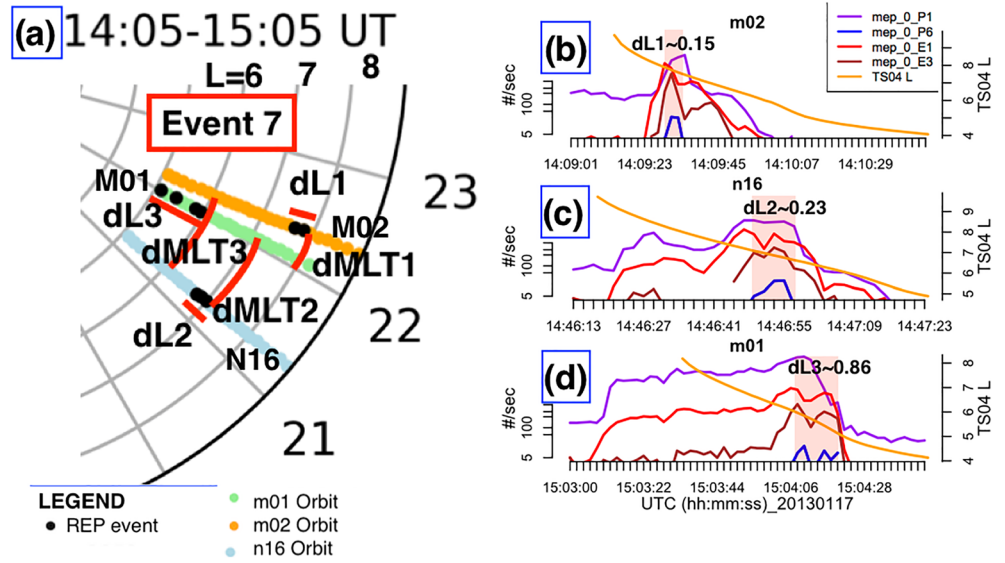


**Figure 7.** (a) L-MLT locations of all POES/MetOp spacecraft between 14:05 to 15:05 UT. Sun is located to the left. Locations are shown for the times of REP observation and POES orbits in the Southern Hemisphere. The region of precipitation was marked by dL and dMLT highlighted in red. MetOp-02, NOAA-16, and MetOp-01 observed REP and the region of precipitation was defined by 3 dLs and 3 dMLTs and are marked in red. (b), (c), and (d) show the REP observations by MetOp-02, NOAA-16, and MetOp-01 at 14:09, 14:46, and 15:04 UT, respectively. In each case, dL is measured as the satellite moves in L shell and sees elevated count rates in the P6 channel (blue).

different locations. Hence, three different regions defined by dL1, dMLT1; dL2, dMLT2; and dL3, dMLT3 were considered.

### 4.3. Net Loss Calculations

The loss of electrons observed by POES/MetOp satellites was quantified using the methodology used by O'Brien et al. (2004) and Blum et al. (2013), where the electrons lost to the atmosphere were calculated using Equation 5.

$$\#e^- = \Delta f \cdot \Delta T \cdot A \cdot 2 \cdot \pi \quad (5)$$

where  $\Delta f$  is the magnitude of the BLC flux,  $\Delta T$  is the duration of the precipitation in hours UT, and  $A$  is the area of the precipitation region at the satellite altitude. A factor of 2 appeared in the study of Blum et al. (2013) where precipitation was assumed to be in conjugate hemispheres, but as seen in Figure 1, in this case, all precipitation events were observed in the Southern Hemisphere only; hence, it was dropped. The factor  $2\pi$  appears from an assumption of isotropy over the downgoing hemisphere. To calculate  $\Delta T$ , we calculated the time interval between the first and the last observation for each REP Events 1, 5, and 7 and for Events 2, 3, 4, and 6, using the time interval between the nearest satellite pass as it crosses the L location of the REP event observed. The latitudes and longitudes at these points were used to define event start latitude/longitude ( $\theta_{start}/\phi_{start}$ ) and end latitudes/longitudes ( $\theta_{end}/\phi_{end}$ ).

Combining Equations 1,3,4, and 5 results in the calculation of number of electrons lost to the atmosphere measured by POES/MetOp. The loss was calculated for each region of precipitation listed in Table 3 and added when they collectively defined an event.

$$\#e^- = \frac{P6_{counts}}{G} \cdot \Delta T \cdot 4 \cdot \pi^2 \cdot (R_E + h)^2 \cdot (\sin(\theta_{end}) - \sin(\theta_{start})) \cdot (\phi_{end} - \phi_{start}) \quad (6)$$

To determine the contribution to global loss of electrons, we calculated the total content of trapped  $>0.7$ -MeV electrons in the outer radiation belt using data from the 90° P6 channel of the MEPED instrument of POES/MetOp around the SAA (South Atlantic Anomaly) region. While at all other longitudes, 90° P6 channel mostly provides drift loss cone flux, around the SAA, it mostly provides trapped flux as drift loss cone (DLC) particles are pushed to BLC in this region (Pham et al., 2017). To calculate trapped flux, as POES moved across L shells of 4–7 around the longitudes of SAA (340° to 360°), we assumed a  $\sin^n \theta$  pitch angle distribution with empirical values of power  $n$  from Vampola (1998). We then integrated over the pitch angle



**Table 3**  
REPs Observed on BARREL Payloads and POES/MetOp on 17 January 2013

REP time and location	REP time and spatial extent	Region of prec.	Electrons lost
Event 1	$\Delta T = 00:16$	Start/end lat = $-76.67^\circ$ , $-76.58^\circ$	$1.5 \times 10^{22}$
NOAA-16	$\Delta L = 0.06$	Start/end lon: $312.19^\circ$ , $284.0^\circ$	
2:44 UT, L: 6.23, MLT = 22.55	$\Delta MLT = 0.85$	$d\theta = 0.09^\circ$ , $d\phi = 28.19^\circ$	
Flux = $1,050 \text{ s}^{-1} \text{ cm}^{-2} \text{ sr}^{-1}$		Area = $5.95 \times 10^{10} \text{ m}^2$	
BARREL 1G			
3:00 UT, L: 6.4, MLT: 21.7			
Flux = $7,467 \text{ s}^{-1} \text{ cm}^{-2} \text{ sr}^{-1}$			
<b>Event 2</b>	$\Delta T = 00:53$	Start/end lat = $-66.62^\circ$ , $-66.71^\circ$	$1.1 \times 10^{22}$
BARREL 1I	$\Delta L = 0.04$	Start/end lon = $202.04^\circ$ , $218.4^\circ$	
4:50 UT, L = 6.6, MLT = 19.5	$\Delta MLT = 2.36$	$d\theta = 0.09^\circ$ , $d\phi = 16.36^\circ$	
Flux = $1,231 \text{ s}^{-1} \text{ cm}^{-2} \text{ sr}^{-1}$		Area = $4.6 \times 10^{10} \text{ m}^2$	
Event 3	$\Delta T = 00:45$	Start/end lat: $-66.88^\circ$ , $-66.94^\circ$	$2.6 \times 10^{20}$
BARREL 1I	$\Delta L = 0.28$	Start/end lon: $199.27^\circ$ , $198.75^\circ$	
8:30–9:15 UT, L = 8.2–8.5, MLT = 23.4–0	$\Delta MLT = 0.65$	$d\theta = 0.048^\circ$ , $d\phi = 0.52^\circ$	
Flux = $1,570 \text{ s}^{-1} \text{ cm}^{-2} \text{ sr}^{-1}$		Area = $9.9 \times 10^8 \text{ m}^2$	
Event 4	$\Delta T = 00:48$	Start/end lat: $-63.25^\circ$ , $-62.69^\circ$	$1.3 \times 10^{23}$
MetOp-01	$\Delta L = 0.31$	Start/end lon: $175.87^\circ$ , $207.51^\circ$	
T = 9:55UT, L = 7.13, MLT = 0.05	$\Delta MLT = 1.95$	$d\theta = 0.56^\circ$ , $d\phi = 31.63^\circ$	
Flux = $900 \text{ s}^{-1} \text{ cm}^{-2} \text{ sr}^{-1}$		Area = $7.8 \times 10^{11} \text{ m}^2$	
<b>Event 5</b>	$\Delta T = 01:41$	Region 1, Region2	$4.7 \times 10^{22}$
NOAA-19	$\Delta L1 = 0.11$	Start lat: $-62.05^\circ$ , $-55.88^\circ$	
11:54 UT, L = 7.06, MLT = 1.73	$\Delta MLT = 0.09$	End lat: $-61.94^\circ$ , $-55.43^\circ$	$5.5 \times 10^{23}$
Flux = $1,100 \text{ s}^{-1} \text{ cm}^{-2} \text{ sr}^{-1}$		$d\theta = 0.11^\circ$ , $0.45^\circ$	Tot = $6 \times 10^{23}$
NOAA-19	$\Delta L2 = 0.42$	Start/end lon = $166.7^\circ$ , $188.07^\circ$	
13:35 UT, L = 6.66, MLT = 1.64		$d\phi = 21.37^\circ$	
Flux = $2,360 \text{ s}^{-1} \text{ cm}^{-2} \text{ sr}^{-1}$		Area 1 = $1.12 \times 10^{11} \text{ m}^2$	
		Area 2 = $5.52 \times 10^{11} \text{ m}^2$	
		Tot = $6.64 \times 10^{11} \text{ m}^2$	
<b>Event 6</b>	$\Delta T = 01:42$	Start lat = $-52.33^\circ$	$9.3 \times 10^{22}$
MetOp-02	$\Delta MLT = 0.57$	End lat = $-52.22^\circ$	
12:27 UT, L = 6.5, MLT = 22.95	$\Delta L = 0.1$	$d\theta = 0.11^\circ$	
Flux = $1,300 \text{ s}^{-1} \text{ cm}^{-2} \text{ sr}^{-1}$		Start lon = $160.32^\circ$	
		End lon = $132.94^\circ$	
		$d\phi = 27.38^\circ$	
		Area = $1.85 \times 10^{11} \text{ m}^2$	
<b>Event 7</b>	$\Delta T = 00:55$	Region 1, Region 2, Region 3	
MetOp-02	$\Delta MLT1 = 0.27$	Start lat = $-48.98^\circ$ , $-48.18^\circ$ , $-46.61^\circ$	$5.4 \times 10^{22}$
14:09 UT, L = 7.8, MLT = 22.34	$\Delta L1 = 0.15$	End lat = $-48.87^\circ$ , $-47.96^\circ$ , $-45.91^\circ$	$3.5 \times 10^{22}$
Flux = $2,700 \text{ s}^{-1} \text{ cm}^{-2} \text{ sr}^{-1}$		$d\theta = 0.11^\circ$ , $0.22^\circ$ , $0.7^\circ$	$2.1 \times 10^{23}$
NOAA-16	$\Delta L2 = 0.23$	Start lon = $119.93^\circ$ , $99.99^\circ$ , $119.93^\circ$	
14:46 UT, L = 6.76, MLT = 21.25	$\Delta MLT2 = 0.82$	End lon = $106.63^\circ$ , $106.35^\circ$ , $99.94^\circ$	Tot = $3 \times 10^{23}$
Flux = $1,770 \text{ s}^{-1} \text{ cm}^{-2} \text{ sr}^{-1}$		$d\phi = 13.3^\circ$ , $6.36^\circ$ , $19.99^\circ$	
MetOp-01	$\Delta L3 = 0.86$	Area 1 = $9.67 \times 10^{11} \text{ m}^2$	
15:04 UT, L = 5.83, MLT = 22.02	$\Delta MLT3 = 1.09$	Area 2 = $9.47 \times 10^{11} \text{ m}^2$	
Flux = $1050 \text{ s}^{-1} \text{ cm}^{-2} \text{ sr}^{-1}$		Area 3 = $9.72 \times 10^{11} \text{ m}^2$	
		Tot = $2.9 \times 10^{12} \text{ m}^2$	

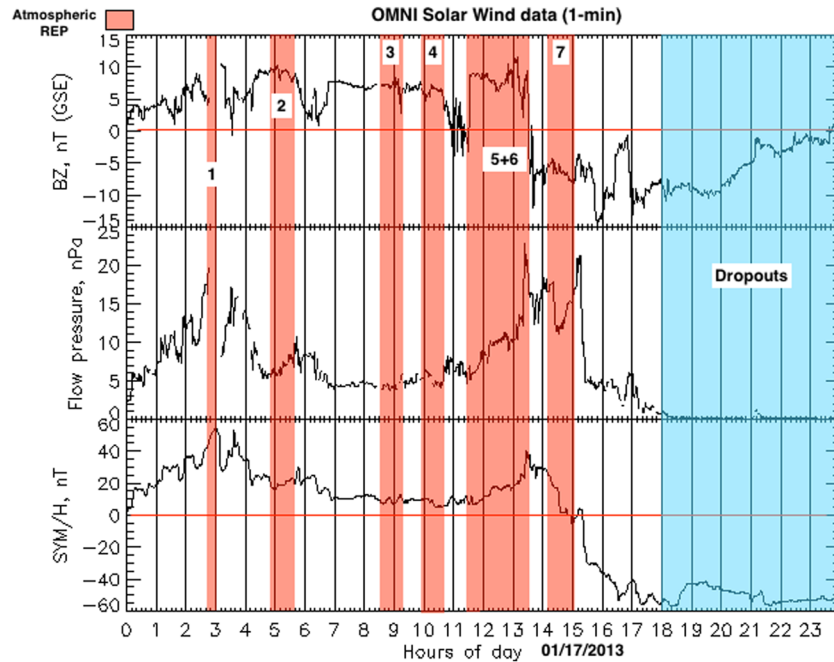


**Figure 8.** Solar wind data on 17 January 2013. It was geomagnetically quite until 14:00 UT around which the geomagnetic activity increased significantly causing minor storm. Times at which atmospheric REP was observed are shown in red. Events 1 to 6 occurred during prestorm times while Event 7 occurred at the commencement of the main phase. The dynamic solar wind pressure was found to peak between 12:00 UT to 16:00 UT, indicating that the magnetopause may have been compressed earthward by the enhanced solar wind pressure leading to magnetopause losses (times shown in blue). Subsequent 2.3-MeV electron dropouts were observed in RBSP A (Figure 9).

distribution and dipole L shell volume to get an estimate of the number of trapped electrons between L shells of 4–7. We estimated the trapped electrons for 10 POES/MetOp passes around SAA between 2:00 to 15:00 UT and picked the mean as the number of electrons trapped. This was estimated to be roughly  $\sim 10^{26}$ . The loss percentage was then calculated as ratio of total number of precipitating electrons and the number of trapped electrons listed in Equation 7.

$$\#e^-_{\text{Trapped}} \sim 10^{26}, \#e^-_{\text{Loss}} \sim 5.4 \times 10^{24} \text{ or } \sim 5.4\% \quad (7)$$

Adding up the contribution from all seven events shows that around 5% of radiation belt was emptied in a duration of  $\sim 13.5$  h on 17 January 2013. Interestingly, Events 1 and 2, which had been previously shown to be caused by EMIC wave-particle scattering through quasilinear simulations by Li et al. (2014) and Woodger et al. (2018), respectively, contributed to roughly less than 1% of the atmospheric loss. We further checked wave data (GOES and ground-based magnetometers) and found that waves were found to be absent for Events 3 and 4 (see Figure 5a in Shprits et al., 2016 for GOES 15 wave data during this time) contributing to roughly 2% of the total atmospheric loss. Wave observations were not available for Events 6 and 7.

#### 4.4. Limitations

Quantification of loss with the SEM 2 MEPED telescopes onboard NOAA POES and EUMETSAT MetOp is subject to a few limitations due to the small field of view of the particle detectors and the spatiotemporal resolution of the atmospheric REP observations. While balloons provide a near-stationary view and hence better estimation of the time duration of REP, POES/MetOp provides better spatial extent estimation as they move faster across L shells and MLTs.

The accuracy of the estimation of particle loss is dependent on the availability of simultaneous balloon and satellite observations, the duration of time spent by the balloons or satellites in the precipitation region, and the spatial resolution of the observations. Further, BARREL measurement would be integrated over the sky, so the location of precipitation could not be constrained in detail contrary to the direct in situ precipitation measurements performed by POES/MetOp. This will affect the determination of spatial scale size of the energetic electron precipitation.

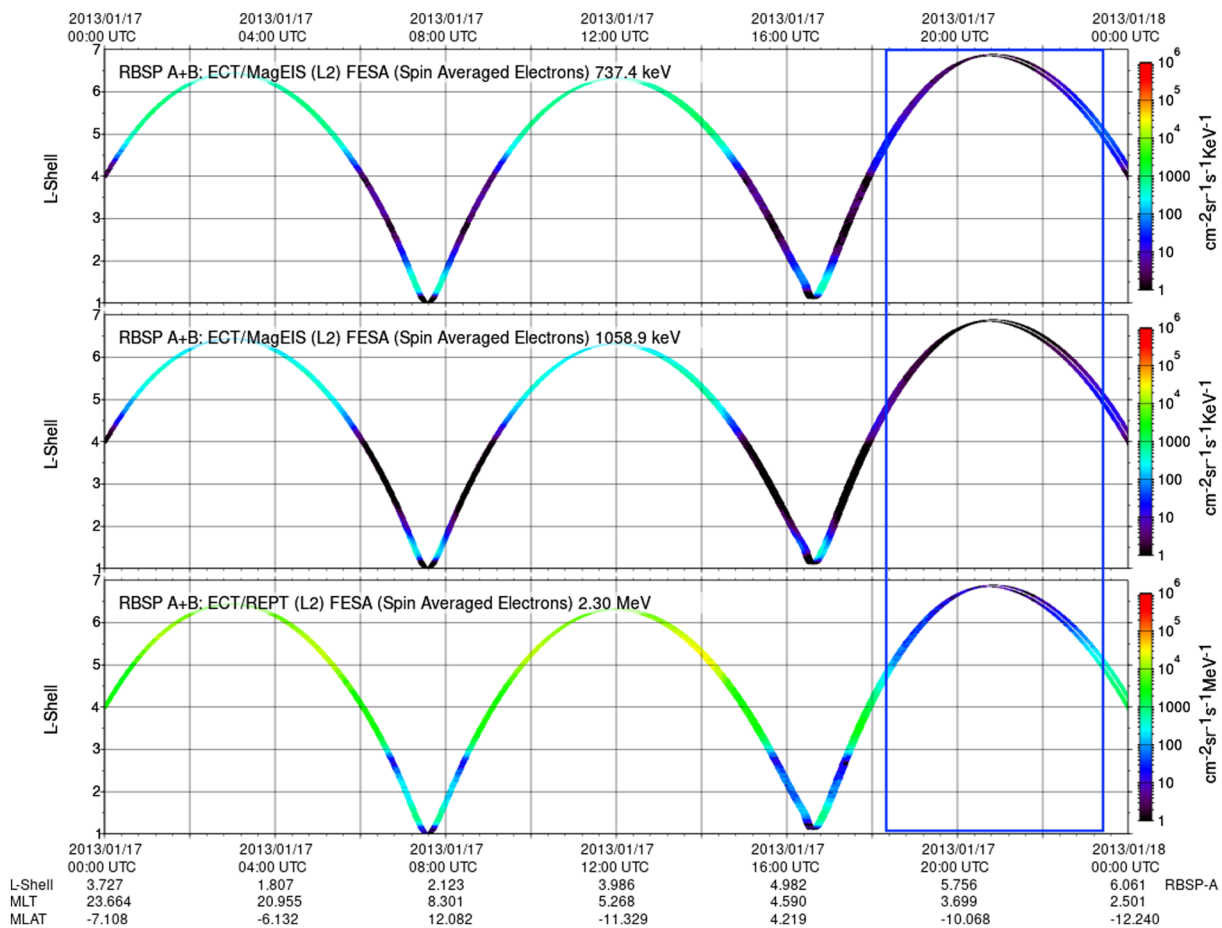


**Figure 9.** RBSP A and B 0.7, 1 and 2.3-MeV electrons flux data on 17 January 2013 (top to bottom). As RBSP A and B move across  $L > 4$  after 16:00 UT, there was a substantial loss of MeV electrons (blue box) in comparison to the fluxes observed by RBSP A before 16:00 UT (<http://rbspgway.jhuapl.edu/>).

Also, MEPED telescopes measure a fraction of particles in the BLC, since the size of telescope field of view is smaller than the BLC which means that weak diffusion events may go undetected (Rodger et al., 2013). This fact may result in not only the underestimation of radiation belt electron loss through precipitation, but also overestimation of the spatial extent of the events due to missed weak events.

For all the observed REP events, lower energy electron precipitation was observed in POES/MetOP satellites in the E3 channel. As discussed by Shekhar et al. (2017), for the MEPED  $0^\circ$  instrument, the count rates in the P6 channel could only be confirmed to be due to BLC particles if the count rates in the E3 channel were greater than the count rates in the P6 channel. The P6 channel may observe high-energy DLC particles penetrating through the sides and back of the instrument rather than aperture. Hence, in order to separate DLC fluxes in the P6 channel from BLC fluxes, E3 channel is required to be checked for precipitation. In this study, we are assuming that the processes responsible for pitch angle scattering MeV electrons may also facilitate precipitation of  $>300$ -keV electrons (Shprits et al., 2009).

### 5. Geomagnetic Conditions and Electron Loss

The solar wind data on 17 January 2013 (Figure 8) showed that it was geomagnetically quiet until 14:00 UT around which the geomagnetic activity increased causing minor storm. Events 1 to 6 occurred during prestorm times while Event 7 occurred at the commencement of the main phase. Quantitatively, almost 75% of atmospheric precipitation occurred during prestorm times.

Atmospheric REPs were not observed by POES/MetOp or BARREL payloads after 15:04 UT. Since POES/MetOp provides coverage over all MLT sectors, it might imply that significant atmospheric precipitation may not have occurred after 15:04 UT. Figure 9 shows RBSP (Radiation Belt Storm Probe) A and B

0.7, 1 and 2.3-MeV electron flux data, indicating that as it moved across  $L > 4$  after 16:00 UT, there was a substantial loss of  $>0.7$ -MeV electrons in comparison to the fluxes observed by RBSP A and B before 16:00 UT. It might imply that this dropout may have been attributed to mechanisms other than those leading to atmospheric precipitation of relativistic electrons. The dynamic solar wind pressure (Figure 8) was found to peak between 12:00 UT to 16:00 UT, indicating that the magnetopause may have been compressed earthward by the enhanced solar wind pressure. These conditions favor loss through magnetopause shadowing (e.g., Li et al., 1997; Matsumura et al., 2011). Turner et al. (2014) showed that this process is important for electron loss at higher L shells.

## 6. Conclusions and Discussions

Several POES/MetOp satellites and BARREL payloads observed REP on 17 January 2013. While previous comparisons of BARREL data on this day with quasilinear diffusion models by Li et al. (2014) and Woodger et al. (2018) have been in agreement with EMIC wave-particle interaction mechanism, a quantitative estimation of the contribution of loss was not performed due to lack of spatial data. We used BARREL and POES/MetOp observations conjunctively at a total of 11 different locations and times in a duration of  $\sim 13.5$  h (from 2:44 UT to 15:04 UT). The results are shown in Table 3. The 11 observations were grouped into multiple observations of seven different events. We quantified the loss for each of those seven events and are summarized in Table 3.

1. A net atmospheric loss of  $\sim 5\%$  of the  $>700$  keV (up to 10 MeV) radiation belt particles was obtained between 2:44 to 15:04 UT ( $\sim 13.5$  h) on 17 January 2013.
2. Almost 75% of the atmospheric precipitation occurred during prestorm times through six REP events (average  $\sim 12\%$  per event) while during the commencement of the storm, one REP event caused 25% of the atmospheric precipitation.
3. The flux dropouts during the main phase of the storm were found to not be due to precipitation to the atmosphere.
4. Events 1 and 2 which had been previously shown to be caused by EMIC wave-particle interaction were estimated to contribute to less than 1% of the total atmospheric loss.

On 17 January 2013, we calculated a net atmospheric loss of  $\sim 5\%$  of radiation belt particles in a duration of 13.5 h. For comparison, a study by Blum et al. (2013) quantified electron loss using BARREL and CSSWE CubeSat data for two REP events observed on 18 and 19 January 2013 and estimated  $\sim 5\%$  loss. Further, Millan et al. (2002) estimated that the MeV precipitation events could empty the outer radiation belts of relativistic electrons in  $\sim 3$  days. While Blum et al. (2013) and Millan et al. (2002) estimated event specific loss due to lower spatial coverage, our study, with better spatial resolution, covered all the REP events occurring over the whole day and is reflective of the global net loss due to the interplay between the various source and loss processes. A recent study by Gokani et al. (2019) showed that atmospheric REP was not the major contributor to the observed dropout event at  $L \sim 4$  that occurred during the St. Patrick's Day storm of March 2015. In this case too, we found that only 5% relativistic electrons were precipitated into the atmosphere while a sudden dropout of MeV electrons was observed during the minor storm where no atmospheric precipitation was observed. It implies that atmospheric precipitation may not have been a major contributor of relativistic electron loss from the outer radiation belts.

Further, in a study by Hyun et al. (2014), 3-day geomagnetically quiet period was analyzed where geosynchronous loss of relativistic electrons was observed and was found to not be associated with magnetopause shadowing. Even on 17 January 2013, we found that majority of particle loss through the atmosphere occurred during prestorm time while during the storm, particle loss occurred through mechanisms other than atmospheric precipitation with conditions favoring magnetopause shadowing. However, the magnetopause is not the only place where the electrons can be lost and not all dropout events can be explained by the magnetopause shadowing alone (Gao et al., 2015; Yuan & Zong, 2013). As seen in Figure 8, there was a gradual increase in the dynamic pressure at around 0 UT and it peaked around 3 UT after which all the events had occurred. The level of increase was comparable ( $\sim 19$  nPa) to the level ( $\sim 23$  nPa) observed during geomagnetic storm after 13 UT. While Events 1–6 may have been driven by the pressure pulse around 3 UT, Event 7 may have been driven by a southward IMF Bz and the pressure pulse between 12 to 16 UT. This is in agreement with Gao et al. (2015) where it was shown that both IMF Bz and dynamic solar wind pressure play a key role in causing dropouts. Our results are also in agreement with statistical studies by Meredith

et al. (2011) and Borovsky and Denton (2010) where the flux dropouts during the main phase of high-speed stream-driven storms were found to not be due to precipitation to the atmosphere.

A recent study by Qin et al. (2018) found that only around 25% of EMIC waves observed on Van Allen Probes between 2013 to 2016 were associated with REP. Woodger et al. (2018) recently showed that background magnetic field may impact resonant interaction of electrons with EMIC waves. It has also been shown in previous studies that cold plasma density can play a significant role in the resonant interaction of EMIC waves with radiation belt electrons (e.g., Gendrin, 1975; Thorne & Kennel, 1971). In our study, waves were found to be absent for Events 3 and 4 contributing to roughly 2% of the total atmospheric loss. Also, contribution to atmospheric loss from Events 1 and 2 that were previously shown to be a result of EMIC wave-particle interaction through quasilinear simulations was less than 1%. This puts the significance of the contribution of EMIC waves toward global loss of electrons from the radiation belts to question. In the future, this method could be used to observationally quantify the atmospheric relativistic electron loss statistically using the POES/MetOp data repository which spans over a solar cycle and compare the loss due to different mechanisms.

### Data Availability Statement

Data set were taken from National Oceanic and Atmospheric Administration (1978): POES Space Environment Monitor, Energetic Particles. National Geophysical Data Center, NOAA. <https://doi.org/10.7289/V5JS9NC6> (<https://satdat.ngdc.noaa.gov/sem/poes/data/raw/ngdc/>). OMNI data were taken from <https://omniweb.gsfc.nasa.gov/>. RBSP data were taken from <http://rbspgway.jhuapl.edu/>. BARREL data are available at [http://barreldata.ucsc.edu/data\\_products/v05/12/](http://barreldata.ucsc.edu/data_products/v05/12/).

### Acknowledgments

This work was supported by grants from NASA LWS grant #NNX08AM58Q and Dartmouth College.

### References

- Blum, L. W., Bonnell, J. W., Agapitov, O., Paulson, K., & Kletzing, C. (2017). EMIC wave scale size in the inner magnetosphere: Observations from the dual Van Allen Probes. *Geophysical Research Letters*, *44*, 1227–1233. <https://doi.org/10.1002/2016GL072316>
- Blum, L. W., Schiller, Q., Li, X., Millan, R., Halford, A., & Woodger, L. (2013). New conjunctive CubeSat and balloon measurements to quantify rapid energetic electron precipitation. *Geophysical Research Letters*, *40*, 5833–5837. <https://doi.org/10.1002/2013GL058546>
- Borovsky, J. E., & Denton, M. H. (2010). Magnetic field at geosynchronous orbit during high-speed stream-driven storms: Connections to the solar wind, the plasma sheet, and the outer electron radiation belt. *Journal of Geophysical Research*, *115*, A08217. <https://doi.org/10.1029/2009JA015116>
- Capannolo, L., Li, W., Ma, Q., Shen, X.-C., Zhang, X.-J., Redmon, R. J., et al. (2019). Energetic electron precipitation: Multievent analysis of its spatial extent during EMIC wave activity. *Journal of Geophysical Research: Space Physics*, *124*, 2466–2483. <https://doi.org/10.1029/2018JA026291>
- Comess, M. D., Smith, D. M., Selesnick, R. S., Millan, R. M., & Sample, J. G. (2013). Duskside relativistic electron precipitation as measured by SAMPEX: A statistical survey. *Journal of Geophysical Research: Space Physics*, *118*, 5050–5058. <https://doi.org/10.1002/jgra.50481>
- Fillius, R. W., & McIlwain, C. E. (1967). Adiabatic betatron acceleration by a geomagnetic storm. *Journal of Geophysical Research*, *72*(15), 4011–4015. <https://doi.org/10.1029/JZ072i015p04011>
- Gao, X., Li, W., Bortnik, J., Thorne, R. M., Lu, Q., Ma, Q., et al. (2015). The effect of different solar wind parameters upon significant relativistic electron flux dropouts in the magnetosphere. *Journal of Geophysical Research: Space Physics*, *120*, 4324–4337. <https://doi.org/10.1002/2015JA021182>
- Gendrin, R. (1975). Is the plasmopause a preferential region for proton precipitation. *Annales Geophysicae*, *31*, 127.
- Gokani, S. A., Kosch, M., Clilverd, M., Rodger, C. J., & Sinha, A. K. (2019). What fraction of the outer radiation belt relativistic electron flux at L 3–4.5 was lost to the atmosphere during the dropout event of the St. Patrick's Day storm of 2015? *Journal of Geophysical Research: Space Physics*, *124*, 9537–9551. <https://doi.org/10.1029/2018JA026278>
- Hyun, K., Kim, K.-H., Lee, E., Kwon, H.-J., Lee, D.-H., & Jin, H. (2014). Loss of geosynchronous relativistic electrons by EMIC wave scattering under quiet geomagnetic conditions. *Journal of Geophysical Research: Space Physics*, *119*, 8357–8371. <https://doi.org/10.1002/2014JA020234>
- Kataoka, R., Asaoka, Y., Torii, S., Terasawa, T., Ozawa, S., Tamura, T., et al. (2016). Relativistic electron precipitation at international space station: Space weather monitoring by calorimetric electron telescope. *Geophysical Research Letters*, *43*, 4119–4125. <https://doi.org/10.1002/2016GL068930>
- Lee, J. J., Parks, G. K., Min, K. W., McCarthy, M. P., Lee, E. S., Park, J. H., & Hwang, J. A. (2006). Relativistic electron dropouts by pitch angle scattering in the geomagnetotail. *Annales Geophysicae*, *24*, 3151–3159.
- Li, Z., Millan, R. M., Hudson, M. K., Woodger, L. A., Smith, D. M., Chen, Y., et al. (2014). Investigation of EMIC wave scattering as the cause for the BARREL 17 January 2013 relativistic electron precipitation event: A quantitative comparison of simulation with observations. *Geophysical Research Letters*, *41*, 8722–8729. <https://doi.org/10.1002/2014GL062273>
- Li, X., Baker, D. N., Temerin, M., Cayton, T. E., Reeves, E. G. D., Christensen, R. A., et al. (1997). Multisatellite observations of the outer zone electron variation during the November 34, 1993, magnetic storm. *Journal of Geophysical Research*, *102*(A7), 14,123–14,140. <https://doi.org/10.1029/97JA01101>
- Lyons, L. R., & Thorne, R. M. (1972). Parasitic pitch angle diffusion of radiation belt particles by ion cyclotron waves. *Journal of Geophysical Research*, *77*, 5608–5616. <https://doi.org/10.1029/JA077i028p05608>
- Matsumura, C., Miyoshi, Y., Seki, K., Saito, S., Angelopoulos, V., & Koller, J. (2011). Outer radiation belt boundary location relative to the magnetopause: Implications for magnetopause shadowing. *Journal of Geophysical Research*, *116*, A06212. <https://doi.org/10.1029/2011JA016575>

- Meredith, N. P., Horne, R. B., Lam, M. M., Denton, M. H., Borovsky, J. E., & Green, J. C. (2011). Energetic electron precipitation during high-speed solar wind stream driven storms. *Journal of Geophysical Research*, *116*, A05223. <https://doi.org/10.1029/2010JA016293>
- Millan, R. M., Lin, R. P., Smith, D. M., Lorentzen, K. R., & McCarthy, M. P. (2002). X-ray observations of MeV electron precipitation with a balloon-borne germanium spectrometer. *Geophysical Research Letters*, *29*(24), 2194. <https://doi.org/10.1029/2002GL015922>
- Millan, R. M., McCarthy, M. P., Sample, J. G., Smith, D. M., Thompson, L. D., McGaw, D. G., et al. (2013). The Balloon Array for RBSP Relativistic Electron Losses (BARREL). *Space Science Reviews*, *179*, 503–530. <https://doi.org/10.1007/s11214-013-9971-z>
- Miyoshi, Y., Sakaguchi, K., Shiokawa, K., Evans, D., Albert, J., Connors, M., & Jordanova, V. (2008). Precipitation of radiation belt electrons by EMIC waves, observed from ground and space. *Geophysical Research Letters*, *35*, L23101. <https://doi.org/10.1029/2008GL035727>
- O'Brien, T. P., Looper, M. D., & Blake, J. B. (2004). Quantification of relativistic electron microburst losses during the GEM storms. *Geophysical Research Letters*, *31*, L04802. <https://doi.org/10.1029/2003GL018621>
- Onsager, T. G., Rostoker, G., Kim, H.-J., Reeves, G. D., Obara, T., Singer, H. J., & Smithtro, C. (2002). Radiation belt electron flux dropouts: Local time, radial, and particle-energy dependence. *Journal of Geophysical Research*, *107*(A11), 1382. <https://doi.org/10.1029/2001JA000187>
- Pham, K. H., Tu, W., & Xiang, Z. (2017). Quantifying the precipitation loss of radiation belt electrons during a rapid dropout event. *Journal of Geophysical Research: Space Physics*, *122*, 10,287–10,303. <https://doi.org/10.1002/2017JA024519>
- Qin, M., Hudson, M., Millan, R., Woodger, L., & Shekhar, S. (2018). Statistical investigation of the efficiency of EMIC waves in precipitating relativistic electrons. *Journal of Geophysical Research: Space Physics*, *123*, 6223–6230. <https://doi.org/10.1029/2018JA025419>
- Rodger, C. J., Clilverd, M. A., Green, J. C., & Lam, M. M. (2010). Use of POES SEM-2 observations to examine radiation belt dynamics and energetic electron precipitation into the atmosphere. *Journal of Geophysical Research*, *115*, A04202. <https://doi.org/10.1029/2008JA014023>
- Rodger, C. J., Kavanagh, A. J., Clilverd, M. A., & Marple, S. R. (2013). Comparison between POES energetic electron precipitation observations and riometer absorptions: Implications for determining true precipitation fluxes. *Journal of Geophysical Research: Space Physics*, *118*, 7810–7821. <https://doi.org/10.1002/2013JA019439>
- Shekhar, S., Millan, R. M., & Hudson, M. K. (2018). A statistical study of spatial variation of relativistic electron precipitation energy spectra with Polar Operational Environmental Satellites. *Journal of Geophysical Research: Space Physics*, *123*, 3349–3359. <https://doi.org/10.1002/2017JA025041>
- Shekhar, S., Millan, R., & Smith, D. (2017). A statistical study of the spatial extent of relativistic electron precipitation with polar orbiting environmental satellites. *Journal of Geophysical Research: Space Physics*, *122*, 11,274–11,284. <https://doi.org/10.1002/2017JA024716>
- Shprits, Y. Y., Chen, L., & Thorne, R. M. (2009). Simulations of pitch angle scattering of relativistic electrons with MLT-dependent diffusion coefficients. *Journal of Geophysical Research*, *114*, A03219. <https://doi.org/10.1029/2008JA013695>
- Shprits, Y. Y., Drozdov, A. Y., Spasojevic, M., et al. (2016). Wave-induced loss of ultra-relativistic electrons in the Van Allen radiation belts. *Nature Communications*, *7*, 12,883. <https://doi.org/10.1038/ncomms12883>
- Smith, D. M., Casavant, E. P., Comess, M. D., Liang, X., Bowers, G. S., Selesnick, R. S., et al. (2016). The causes of the hardest electron precipitation events seen with SAMPEX. *Journal of Geophysical Research: Space Physics*, *121*, 8600–8613. <https://doi.org/10.1002/2016JA022346>
- Summers, D., & Thorne, R. M. (2003). Relativistic electron pitch-angle scattering by electromagnetic ion cyclotron waves during geomagnetic storms. *Journal of Geophysical Research*, *108*(A4), 1143. <https://doi.org/10.1029/2002JA009489>
- Thorne, R. M., & Kennel, C. F. (1971). Relativistic electron precipitation during magnetic storm main phase. *Journal of Geophysical Research*, *4446–4453*(19). <https://doi.org/10.1029/JA076i019p04446>
- Tu, W., Selesnick, R., Li, X., & Looper, M. (2010). Quantification of the precipitation loss of radiation belt electrons observed by SAMPEX. *Journal of Geophysical Research*, *115*, A07210. <https://doi.org/10.1029/2009JA014949>
- Turner, D. L., et al. (2014). On the cause and extent of outer radiation belt losses during the 30 September 2012 dropout event. *Journal of Geophysical Research: Space Physics*, *119*(1530–1540). <https://doi.org/10.1002/2013JA019446>
- Ukhorskiy, A. Y., Shprits, Y. Y., Anderson, B. J., Takahashi, K., & Thorne, R. M. (2010). Rapid scattering of radiation belt electrons by storm time EMIC waves. *Geophysical Research Letters*, *37*, L09101. <https://doi.org/10.1029/2010GL042906>
- Vampola, A. L. (1998). Outer zone energetic electron environment update. In *Proceedings of the conference on the high energy radiation background in space: Snowmass*, IEEE Conference Proceedings, CO, USA, pp. 128–136.
- Woodger, L. A., Halford, A. J., Millan, R. M., McCarthy, M. P., Smith, D. M., Bowers, G. S., et al. (2015). A summary of the BARREL campaigns: Technique for studying electron precipitation. *Journal of Geophysical Research: Space Physics*, *120*, 4922–4935. <https://doi.org/10.1002/2014JA020874>
- Woodger, L. A., Millan, R. M., Li, Z., & Sample, J. G. (2018). Impact of background magnetic field for EMIC wave-driven electron precipitation. *Journal of Geophysical Research: Space Physics*, *123*, 8518–8532. <https://doi.org/10.1029/2018JA025315>
- Yando, K., Millan, R. M., Green, J. C., & Evans, D. S. (2011). A Monte Carlo simulation of the NOAA POES Medium Energy Proton and Electron Detector instrument. *Journal of Geophysical Research*, *116*, A10231. <https://doi.org/10.1029/2011JA016671>
- Young, S. L., Denton, R. E., Anderson, B. J., & Hudson, M. K. (2002). Empirical model for scattering caused by field line curvature in a realistic magnetosphere. *Journal of Geophysical Research*, *107*(A6), SMP 3–1–SMP 3–9. <https://doi.org/10.1029/2000JA000294>
- Yuan, C. J., & Zong, Q. G. (2013). Relativistic electron fluxes dropout in the outer radiation belt under different solar wind conditions. *Journal of Geophysical Research: Space Physics*, *118*, 7545–7556. <https://doi.org/10.1002/2013JA019066>
- Zhang, K., Li, X., Schiller, Q., Gerhardt, D., Zhao, H., & Millan, R. (2017). Detailed characteristics of radiation belt electrons revealed by CSSWE/REPTile measurements: Geomagnetic activity response and precipitation observation. *Journal of Geophysical Research: Space Physics*, *122*, 8434–8445. <https://doi.org/10.1002/2017JA024309>